Covalent chemistry on a van der Waals heterostructure

Julia Villalva,[a] Sara Moreno,[a] Palmira Villa,[b] Luisa Ruiz-González,[c] Cristina Navio,[a] Andres Castellanos-Gomez,[d] Emerson Giovanelli,[a] and Emilio M. Pérez*[a]

[a] IMDEA Nanociencia; c/ Faraday 9, Campus de Cantoblanco; 28049 Madrid, Spain.
Twitter: @emiliomperezlab
E-mail: emilio.perez@imdea.org
[b] Instituto Pluridisciplinar; Universidad Complutense de Madrid; Paseo de Juan XXIII Nº 1, 28040 Madrid, Spain.
[c] Departamento de Química Inorgánica; Universidad Complutense de Madrid, Av. Complutense s/n, 28040 Madrid, Spain.
[d] Instituto de Ciencia de Materiales de Madrid (ICMM-CSIC), Sor Juana Inés de la Cruz, 3, Campus de Cantoblanco, 28049 Madrid, Spain.

Abstract: The building of van der Waals heterostructures[1, 2, 3, 4, 5, 6, 7] and the decoration of 2D materials with organic molecules[8, 9, 10] share a common goal: to obtain ultrathin materials with tailored properties.[11, 12, 13, 14, 15, 16, 17] Performing controlled chemistry on van der Waals heterostructures would add an extra level of complexity, providing a pathway towards 2D-2D-0D mixed-dimensional heterostructures. Here we show that thiol-ene-like “click” chemistry[18, 19] can be used to decorate franckeite,[20, 21, 22, 23] a naturally occurring van der Waals heterostructure with maleimide reagents. ATR-IR and NMR analyses corroborate the Michael addition mechanism via the formation of a S−C covalent bond, while Raman and HR-TEM show that the SnS_2-PbS alternating structure of franckeite is preserved, and suggest that SnS_2 reacts preferentially, which is confirmed through XPS. We illustrate how this methodology can be used to add functional molecular moieties by decorating franckeite with porphyrins. UV-vis-NIR spectroscopy confirms that the chromophore remains operative and shows negligible electronic interactions with franckeite in the ground state, while its fluorescence is strongly quenched upon photoexcitation.

Introduction: The stack of different 2D materials is the root of the field of van der Waals heterostructures.[1, 2, 3] The most widespread method for the synthesis of heterostructures of bidimensional materials is the direct growth of one material on top of the other by CVD, or van der Waals[4] or edge[5] epitaxy. Alternatively, one can manually stack one material on top of the other, using deterministic transfer methodologies.[6, 7] This is usually done by using a viscoelastic polymer as transfer media, on which one of the flakes is adhered and then placed on top of the other using optical microscopy and spectroscopy to monitor the alignment.[24] Alternatively, one can obtain ultrathin van der Waals heterostructures from the direct exfoliation of minerals of adequate composition.[20, 21, 22, 23, 25, 26, 27, 28] The motivation behind this field of research is based on the expectation that the combination (or modulation) of properties of nanomaterials is a promising approach towards materials by design.[11, 12, 13, 14, 15, 16, 17] This exact same motivation fuels the interest in the chemistry of 2D materials:[8, 9] we expect that the decoration of the nanomaterials with functional molecular fragments will yield superior combined properties.[10] Besides this application-oriented point of view, the chemistry of 2D materials presents very interesting fundamental challenges, like obtaining chemical selectivity in materials where most atoms are chemically identical.[29, 30] To the best of our knowledge, the covalent chemistry of van der Waals heterostructures is still unexplored territory.

With these considerations in mind, we decided to explore the chemistry of a naturally occurring van der Waals heterostructure: franckeite. Franckeite (Fk) is composed of the alternate layers of one pseudohexagonal (H) tin(IV) sulfide (SnS_2)-like layer and four pseudotetragonal (T) lead(II) sulfide (PbS)-like layers (Figure 1a).[31] Among its attractive features, we can highlight that Fk is an air-stable semiconductor with a very

small bandgap (0.5-0.7 eV) and presents p-type doping, mostly due to substitutional Sb(III) in the structure.[32]

We have very recently reported the use of thiol-maleimide "click" chemistry[18, 19] to functionalize MoS_2 and WS_2 under particularly mild conditions.[33] We believed this powerful reaction would be an ideal tool to take the first steps towards heterostructures of the 2D-2D-0D type, where the 0D material are functional organic molecules. From the fundamental chemistry point of view, we wanted to address the possibility of performing thiol-maleimide chemistry on a material composed of two different sulfides. Here, we describe how to functionalize Fk covalently using maleimides as soft electrophiles. At room temperature in isopropanol (iPrOH), we achieve preferential reactivity of the sulfides in the SnS_2 layer to form S–C bonds, with sufficient selectivity to conserve the van der Waals heterostructure. As proof-of-principle application, we describe the functionalization of Fk with a porphyrin-decorated maleimide.

Results and discussion:

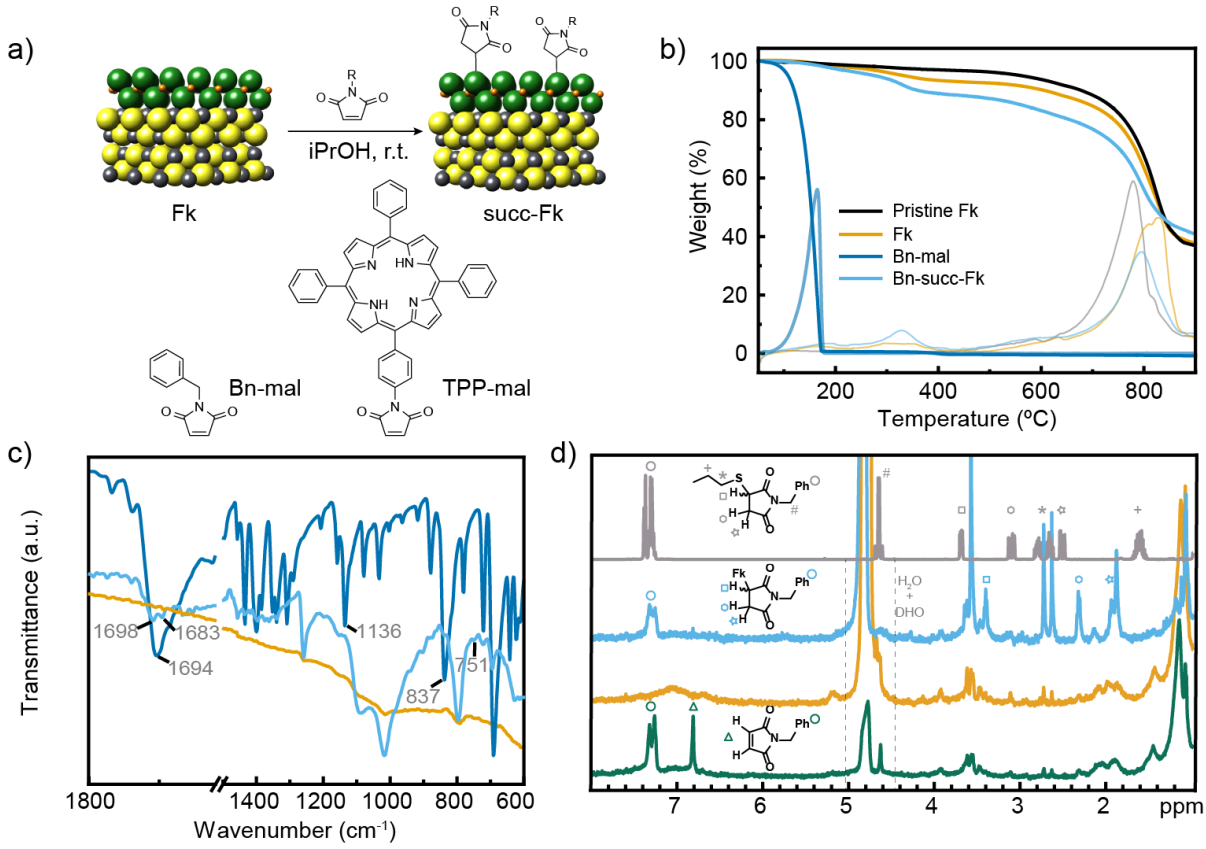

Figure 1. a) Chemical structure of Fk from its X-ray crystal structure,[31] and idealized reaction scheme with maleimides. Based on HR-TEM and XPS data we show SnS_2 as the reactive layer. The S atoms in the SnS_2-like layers are green, S atoms in the PbS-like layer are yellow, Sn atoms are orange and Pb atoms are gray. The structures of the two maleimide reagents are also shown. b) TGA (N_2, 10 °C·min^{-1}) of pristine exfoliated Fk (black), control Fk (yellow), Bn-maleimide (intense blue) and functionalized Bn-succ-Fk (pale blue). The first derivatives are shown in thinner lines. c) Comparison of the ATR-IR spectra of control Fk, Bn-maleimide and functionalized Bn-succ-Fk (same colour code as in b). d) HR-MAS-^{1}H-NMR (500 MHz) spectra of Bn-succ-Fk (pale blue), control Fk (orange) and a mixture of Fk and Bn-maleimide (dark green) obtained using D_2O as the reference. The solution ^{1}H NMR ($CDCl_3$, 400 MHz, r.t.) of the product of the reaction between 1-propanethiol and *N*-benzylmaleimide is also shown for comparison (gray).

The structure of Fk and the idealized reaction scheme are shown in Figure 1a. For simplicity, only a minimal repetition unit is drawn. Few-layer Fk colloids were obtained using the liquid-phase exfoliation method previously described.[34] Briefly, Fk powder obtained from careful grinding of mineral pieces was bath ultrasonicated in iPrOH (10 $mg \cdot mL^{-1}$) at 20 °C for 1 h. The colloid obtained in the supernatant after centrifugation at 988 g for 30 min presented a homogeneous distribution of flakes, most of them having a few-layer thickness (<7.5 nm from AFM data, S4). To this colloid, *N*-benzylmaleimide (Bn-mal in Figure 1) was added, and the mixture was ultrasonicated for 5 min then stirred overnight. As for the purification procedure, the suspension was filtered through a polytetrafluoroethylene membrane with a pore size of 0.2 μm, and the solid was washed several times with $CHCl_3$ to remove excess reagents and physisorbed maleimide, $CHCl_3$ was selected after an optimization process as the best washing solvent due to its ability to dissolve Bn-mal. The purification process was monitored by UV-Vis spectroscopy (see S5).

Using thermogravimetric analysis (TGA) the functionalization was estimated at *ca*. 7 wt.% for the Bn-mal and *ca*. 4 wt.% when the porphyrin-derived maleimide (TPP-mal) was employed (Figure 1b and S6). For a rigorous analysis, a control Fk sample was stirred overnight and rinsed afterwards with $CHCl_3$ following the exact same procedure described for the functionalization. This control sample presents an initial weight loss at around 300 °C which can correspond to adsorbed solvent; then it is thermally stable until 700 °C, where it starts to decompose. The organic material loss overlaps that of the solvent but is displaced to much higher temperatures (from 155 °C to 310 °C in Bn-succ-Fk and from 460 °C to 560 °C in TPP-succ-Fk). This improved thermal stability is a first indication that the organic material is not simply physisorbed onto the surface but forming covalent bonds. The low degree of functionalization

compared to MoS_2 and WS_2 under similar reaction conditions[33] is rationalized as a direct consequence of the structure of Fk (see below).

ATR-FTIR shows the presence of new vibration bands in the Bn-succ-Fk sample (Figure 1c). The intense carbonyl stretch that appears at 1694 cm^{-1} in the Bn-mal splits into two new bands in the functionalized sample (1698 and 1683 cm^{-1}). This can be explained by the desymmetrization of the molecule after functionalization. Additionally, the intense alkene C–H bending mode at 837 cm^{-1} is strongly depleted after functionalization, which is in accordance with the expected Michael addition mechanism. We assign the new 751 cm^{-1} weak band, absent in the reference Fk material and in Bn-mal, to the new C–S stretching vibration.

Conclusive evidence about the functionalization and the functionalization mechanism is obtained when the powder sample is analysed using High-Resolution Magic Angle Spinning (HR-MAS) NMR. HR-MAS ^{1}H NMR spectroscopy permits the direct analysis of heterogeneous samples, such as tissue[35] or materials,[36] and has previously been used to track organic reactions in the solid state.[37] Using deuterated water as the reference, the control Fk sample (orange in Figure 1d) shows only weak signals in the alkane region, probably due to adsorbed hydrocarbons and residual iPrOH, and a broad a very weak signal centered around 7 ppm (most likely physisorbed iPrO<u>H</u>). In contrast, the benzylsuccinimide signals are clearly observed in the functionalized Bn-succ-Fk (blue in Figure 1d), which can be unambiguously assigned to covalent functionalization of Fk through Michael addition by comparison with a Fk and *N*-benzylmaleimide mixture (green in Figure 1d): the total depletion of the alkene signals at around 6.8 ppm (green triangle, *ca*. 6.8 ppm) is accompanied by the appearance of three new signals (marked with a square at ca. 3.4 ppm, an hexagon at *ca*. 2.3 ppm, and star at *ca*. 1.9 ppm, in Figure 1d) in the alkane region. The new signals correspond to the new aliphatic

diastereotopic protons of the newly formed succinimide. Comparison with the experimental ^{1}H solution NMR spectrum of the product of the reaction between 1-propanethiol and *N*-benzylmaleimide ($CDCl_3$, 400 MHz, r.t., gray in Figure 1d), where the signals can be unambiguously assigned, further confirms this observation: a consistent upfield shift is observed for all the succinimide signals due to the presence of Fk, while the aromatic protons, initially oriented away from Fk, are hardly affected. Unfortunately, the benzylic $-CH_2$ cannot be reliably identified in the different Fk samples, as spectra were acquired with water suppression.

With the reaction effectiveness and mechanism clearly established, we went on to investigate if/how the Fk structure and electronic properties were affected by the covalent modification. To this end, Raman spectroscopy provided valuable information. Both control and functionalized samples exhibit very similar spectra, with the characteristic Fk Raman peaks (Figure S7 and S8). In particular, we observe a band centered at 86 cm^{-1}, which results from the spheroidal and transverse acoustic phonon modes of the PbS layers. The band at 141 cm^{-1} is assigned to a combination of the 2nd order effect of the SnS_2 layers and the transverse optical and acoustic phonon modes of the PbS layers. The outcome of the longitudinal optical phonon mode of the PbS layers and the atomic orbital E_g of the SnS_2 layers is the band at 201 cm^{-1}. The band at 253 cm^{-1} is the combination of the phonon modes of both layers, PbS and SnS_2, and therefore its relative intensity is a good indication that the thickness of the unique 2D-2D heterostructure is preserved upon functionalization. The A_{1g} mode of SnS_2 results in the formation of the band at 318 cm^{-1}. Finally, the shoulder from ~400 to 650 cm^{-1} shows the longitudinal optical phonon modes of PbS and a 2nd order effect from the SnS_2 layers.[20]

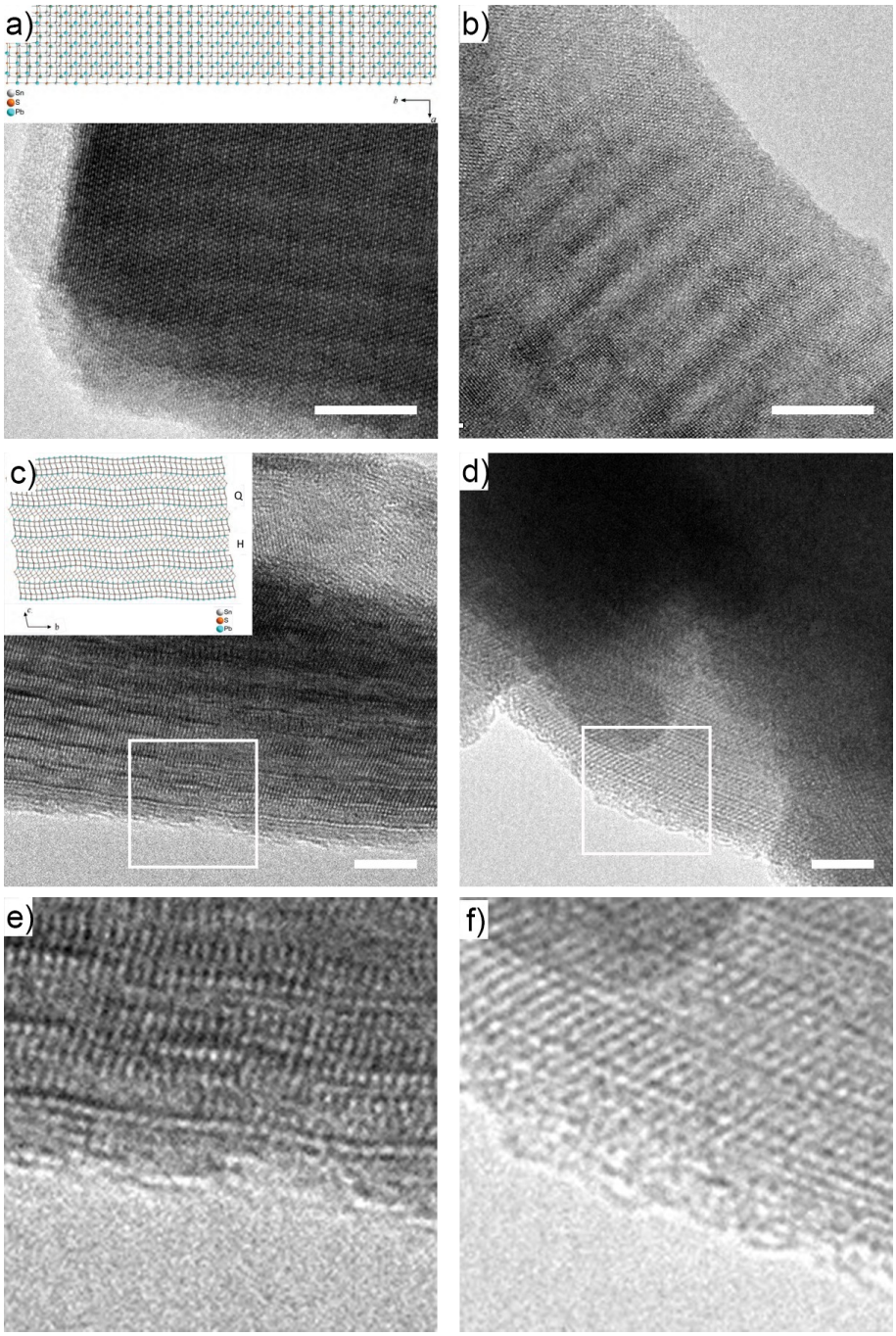

Figure 2. HR-TEM micrographs obtained for pristine Fk (a, c and e) and Bn-succ-Fk (b, d and f). The insets show the orientations that originate the Moiré pattern in a an b, and the edge-on perspective of c and d.[31] Scale bars are 10 nm for a and b and 5 nm for c and d. e) and f) show a zoom in on the edge areas highlighted with white squares in c) and d), respectively.

In agreement with the Raman measurements, high-resolution transmission electron microscopy HRTEM (200 kV) shows no major changes in the van der Waals heterostructure during functionalization. Figures 2a and 2b show the comparison of characteristic micrographs for Fk and Bn-succ-Fk along the [100] direction (see inset).[31] In both micrographs, the same Moiré pattern is observed, which originates from the superposition of the H (SnS_2) and Q (PbS) layers. Figures 2c and 2d, correspond to an edge-on perspective of both samples. The measured periodicities, as better observed in the enhanced details (Figures 2e and 2f), are in agreement with the stacking of the H and Q layers of the Franckeite lattice. A closer look at the final layer (Figures 2e and 2f) suggests that the H layer, i.e., SnS_2, as proved by Velicky et al. [10], is the one exposed to ambient and is therefore most probably the one that reacts preferentially. This is consistent with the chemical intuition based on the lower electronegativity of Sn compared to Pb, and the smaller radius and higher charge of Sn(IV) compared to Pb(II): the combination of these properties should render SnS_2 more purely ionic compared to PbS[38] and, as a consequence, the sulfur atoms directly attached to Sn more anionic and more nucleophilic. This hypothesis also explains the low degree of functionalization observed, as for every potentially reactive SnS_2 layer, there are four PbS layers that remain fundamentally intact. Additionally, the amorphous layer due to organic material appears thicker in Bn-succ-Fk, in accordance with functionalization, although this last observation is far from being conclusive.

To further investigate this point, we have performed X ray Photoelectron Spectroscopy (XPS) measurements under Ultra High Vacuum (UHV) conditions (see the Supporting Information for experimental details). The C 1s core level centered in 284.6 eV was used as a binding energy reference and the selected regions of S 2p, Pb 4f and Sn 3d are shown in Figure 3. With the known structure of franckeite, we would expect for the

valence states of the pristine material to show two different chemical environments for S (one related to the Q type and another to the H type), one for the Pb (related to the Q layer) and two for the Sn (one related to the Q type and another to the H type). In Figure 3 a-c we show the core levels for the S 2p, Pb 4f and Sn 3d for the franckeite control sample. The fit of the S 2p region shows two clear doublets with the $2p_{3/2}$ level centered at 160.5 eV and 161.5 eV. The proportion of the area for each doublet can help on the labeling of the components: as the Q layer is composed by four atomic layers with S, the intensity of this component in the S 2p core level is expected to be larger than for the H layer. We therefore assign the component at 160.5 eV to the Q layer and the one centered in 161.5 eV to the H layer. For the Pb 4f case (Figure 3b) we observe two chemical states instead of one, the Pb^{2+} expected for the Q layer and the appearance of a Pb^{4+} component that can be attributed to the appearance of lead oxide.[20] For the Sn 3d we only observe one chemical state for the franckeite control, which shows the Sn 3d5/2 centered at 485.8 eV.

After functionalization we observe some changes on the XPS spectra, shown in Figure 3d-f. Due to the formation of a C–S bond, a third component could be expected in the S 2p region, but the low degree of functionalization together with limitations on the resolution of XPS make this new chemical state overlap with the components for the franckeite control.[39] This is reflected as a change in the relative atomic percentage in the area of the S 2p. The evidence of the functionalization in the XPS spectra (apart from the appearance of a very weak N 1s peak) is the new component in the Sn 3d region (Figure 3f) located in 487.4 eV, which amounts to 7% of the total area, in good agreement with the degree of functionalization determined by TGA, and is again in support of preferential reaction of the SnS_2 layers.

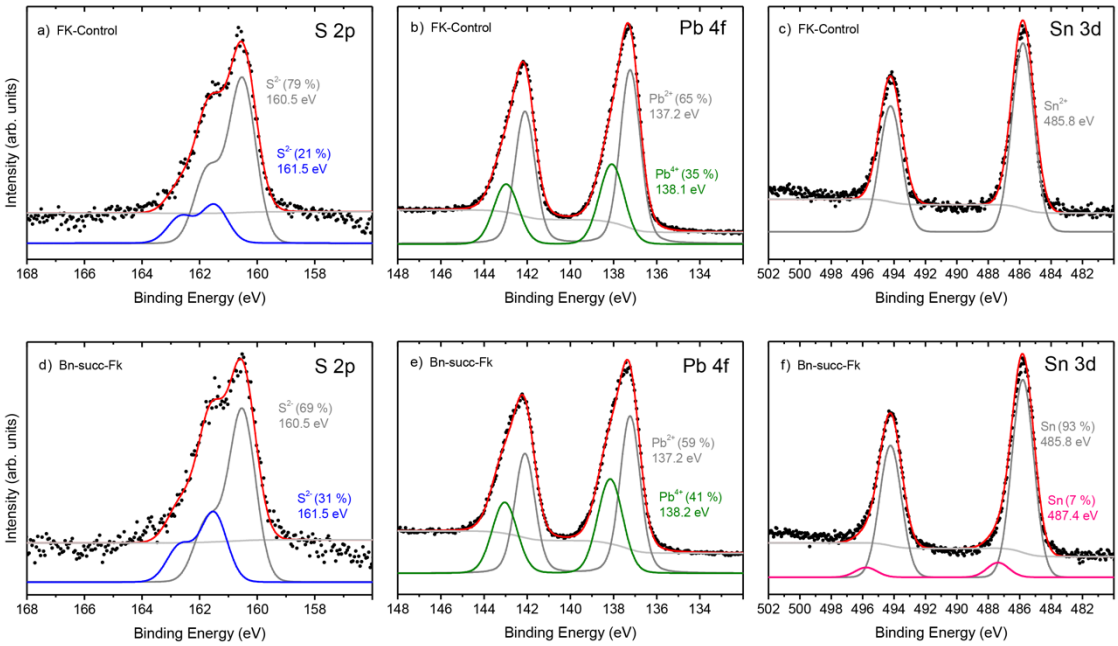

Figure 3. XPS spectra of S, Pb and Sn core levels for (a–c) the control Fk material and (d–f) Bn-succ-Fk.

As proof-of-principle application of our methodology, a maleimide (TPP-mal) bearing a tetraphenylporphyrin TPP group as a chromophore was employed in the reaction. In this case, a clear sign of functionalization is observed in the UV-Vis spectra of the TPP-succ-Fk sample (Figure 4a). The Soret band of the porphyrin core (415 nm in TPP-mal) is without a doubt responsible for the new absorption band observed in TPP-succ-Fk at 417 nm. The very small red shift suggests negligible ground-state electronic interactions.

The photoluminescence emission-excitation maps obtained for TPP-succ-Fk present the distinct Soret and Q bands (Figure 4c, see the PLE map of TPP-mal in Figure 4d as reference), demonstrating again the integrity of the chromophore upon covalent functionalization with Fk. Quantitatively, when the intensities are compared, a clear quenching – by approximately a factor 15 – is observed in the porphyrin emission when

attached to Fk (Figure 4b). This effective quenching is most likely due to photoinduced electron/energy transfer from the TPP group to Fk.

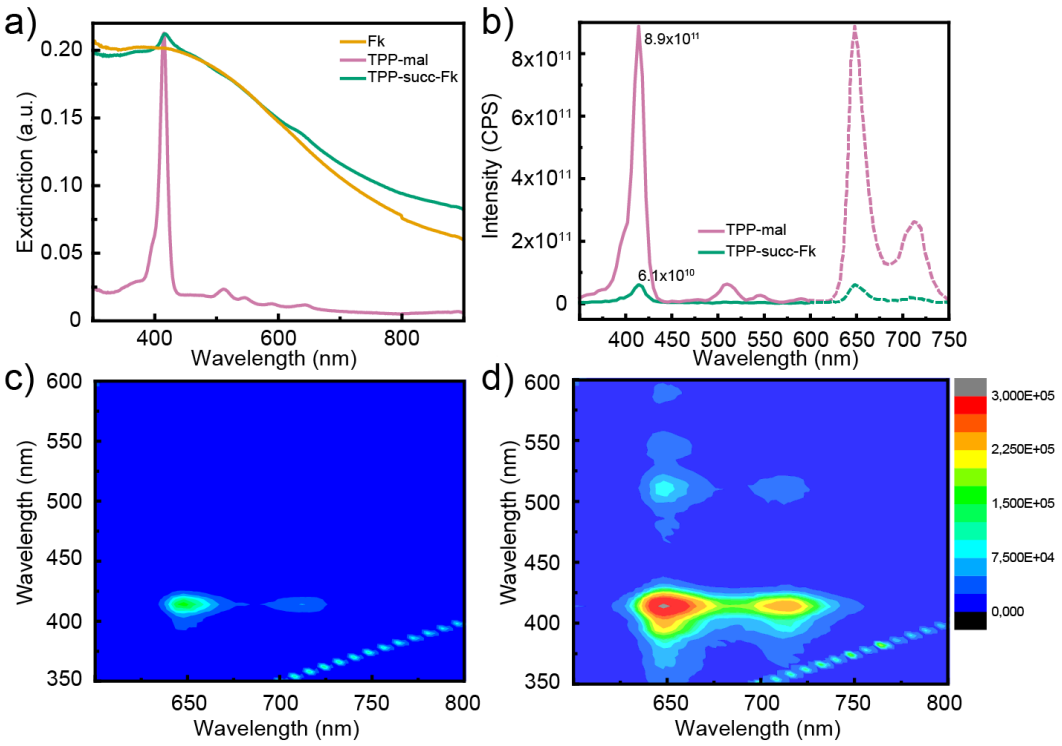

Figure 4. a) UV-Vis spectra of the control Fk sample, tetraphenylporphyrin-derived maleimide (TPP-mal) and TPP-succ-Fk. b) Fluorescence excitation (solid lines) and emission (dashed lines) spectra of TPP-mal and TPP-succ-Fk. c and d) PLE intensity maps of (c) TPP-succ-Fk and (d) TPP-mal. Rayleigh scattering has not been filtered. All spectra were recorded in iPrOH at room temperature.

In conclusion, we describe how the naturally occurring van der Waals heterostructure Fk can be functionalized covalently making use of the inherent soft electrophilicity of maleimides.[33] The good quality of the ^{1}H HR-MAS NMR signals allows us to confirm the proposed thiol-maleimide “click” functionalization mechanism beyond reasonable doubt, and serves as an encouraging example for the use of NMR techniques for the characterization of 2D materials.[40] HR-TEM and XPS confirm that the functionalization

is sufficiently mild to respect the native van der Waals heterostructure, occurring preferentially at the SnS_2 layer.

Finally, we prove that this reaction can be used to connect functional organic molecules by successfully attaching a porphyrin derivative. The steady-state photophysical properties of the 2D-2D-0D mixed-dimensional heterostructure obtained show that the organic chromophore retains its optical properties, with small electronic interactions with the van der Waals heterostructure in the ground state but very effective quenching of the fluorescence upon photoexcitation.

Acknowledgements

We acknowledge funding from the European Union (ERC-StG-307609), MINECO (CTQ2014-60541-P and CTQ2017-86060-P), and the Comunidad de Madrid and the European Structural Funds for their financial support through FotoArt-CM project (S2018/NMT-4367) and MAD2D-CM S2013/MIT-3007. IMDEA Nanociencia acknowledges support from the "Severo Ochoa" Programme for Centres of Excellence in R&D (MINECO, grant SEV-2016-0686).

References

1. Liu Y, Weiss NO, Duan X, Cheng H-C, Huang Y, Duan X. Van der Waals heterostructures and devices. *Nat Rev Mater* 2016, **1:** 16042.
2. Novoselov KS, Mishchenko A, Carvalho A, Castro Neto AH. 2D materials and van der Waals heterostructures. *Science* 2016, **353**(6298).
3. Geim AK, Grigorieva IV. Van der Waals heterostructures. *Nature* 2013, **499**(7459)**:** 419-425.
4. Robinson JA. Growing Vertical in the Flatland. *ACS Nano* 2016, **10**(1)**:** 42-45.
5. Sahoo PK, Memaran S, Xin Y, Balicas L, Gutierrez HR. One-pot growth of two-dimensional lateral heterostructures via sequential edge-epitaxy. *Nature* 2018, **553**(7686)**:** 63-67.
6. Castellanos-Gomez A, Buscema M, Molenaar R, Singh V, Janssen L, van der Zant HSJ, *et al.* Deterministic transfer of two-dimensional materials by all-dry viscoelastic stamping. *2D Mater* 2014, **1**(1)**:** 011002/011001-011002/011008, 011008 pp.

7. Frisenda R, Navarro-Moratalla E, Gant P, Perez De Lara D, Jarillo-Herrero P, Gorbachev RV, *et al.* Recent progress in the assembly of nanodevices and van der Waals heterostructures by deterministic placement of 2D materials. *Chem Soc Rev* 2018, **47**(1)**:** 53-68.
8. Hirsch A, Hauke F. Post-Graphene 2D Chemistry: The Emerging Field of Molybdenum Disulfide and Black Phosphorus Functionalization. *Angew Chem, Int Ed* 2017, **57**(16)**:** 4338-4354.
9. Bertolazzi S, Gobbi M, Zhao Y, Samori P, Backes C. Molecular chemistry approaches for tuning the properties of two-dimensional transition metal dichalcogenides. *Chem Soc Rev* 2018, **47**(17)**:** 6845-6888.
10. Coronado E, Martí-Gastaldo C, Navarro-Moratalla E, Burzurí E, Camón A, Luis F. Hybrid Magnetic/Superconducting Materials Obtained by Insertion of a Single-Molecule Magnet into TaS2 Layers. *Adv Mater* 2011, **23**(43)**:** 5021-5026.
11. Zhang K, Zhang T, Cheng G, Li T, Wang S, Wei W, *et al.* Interlayer Transition and Infrared Photodetection in Atomically Thin Type-II MoTe2/MoS2 van der Waals Heterostructures. *ACS Nano* 2016, **10**(3)**:** 3852-3858.
12. Zhang H, Zhang X, Liu C, Lee S-T, Jie J. High-Responsivity, High-Detectivity, Ultrafast Topological Insulator Bi2Se3/Silicon Heterostructure Broadband Photodetectors. *ACS Nano* 2016, **10**(5)**:** 5113-5122.
13. Massicotte M, Schmidt P, Vialla F, Schadler KG, Reserbat-Plantey A, Watanabe K, *et al.* Picosecond photoresponse in van der Waals heterostructures. *Nat Nanotechnol* 2016, **11**(1)**:** 42-46.
14. Long M, Liu E, Wang P, Gao A, Xia H, Luo W, *et al.* Broadband Photovoltaic Detectors Based on an Atomically Thin Heterostructure. *Nano Lett* 2016, **16**(4)**:** 2254-2259.
15. Mudd GW, Svatek SA, Hague L, Makarovsky O, Kudrynskyi ZR, Mellor CJ, *et al.* High Broad-Band Photoresponsivity of Mechanically Formed InSe-Graphene van der Waals Heterostructures. *Adv Mater* 2015, **27**(25)**:** 3760-3766.
16. Wang L, Zheng X, Chen L, Xiong Y, Xu H. Van der Waals Heterostructures Comprised of Ultrathin Polymer Nanosheets for Efficient Z-Scheme Overall Water Splitting. *Angew Chem, Int Ed* 2018, **57**(13)**:** 3454-3458.
17. Jiang S, Shan J, Mak KF. Electric-field switching of two-dimensional van der Waals magnets. *Nat Mater* 2018, **17**(5)**:** 406-410.
18. Kade MJ, Burke DJ, Hawker CJ. The power of thiol-ene chemistry. *J Polym Sci, Part A: Polym Chem* 2010, **48**(4)**:** 743-750.
19. Hoyle CE, Bowman CN. Thiol-Ene Click Chemistry. *Angew Chem, Int Ed* 2010, **49**(9)**:** 1540-1573.
20. Molina-Mendoza AJ, Giovanelli E, Paz WS, Nino MA, Island JO, Evangeli C, *et al.* Franckeite as a naturally occurring van der Waals heterostructure. *Nature Communications* 2017, **8:** 14409.
21. Velický M, Toth PS, Rakowski AM, Rooney AP, Kozikov A, Woods CR, *et al.* Exfoliation of natural van der Waals heterostructures to a single unit cell thickness. *Nat Commun* 2017, **8:** 14410.
22. Gusmão R, Sofer Z, Luxa J, Pumera M. Layered franckeite and teallite intrinsic heterostructures: shear exfoliation and electrocatalysis. *Journal of Materials Chemistry A* 2018, **6**(34)**:** 16590-16599.
23. Gan S, Zhao Y, Dai X, Xiang Y. Sensitivity enhancement of surface plasmon resonance sensors with 2D franckeite nanosheets. *Results in Physics* 2019, **13:** 102320.

24. Kim K, Yankovitz M, Fallahazad B, Kang S, Movva HCP, Huang S, *et al.* van der Waals Heterostructures with High Accuracy Rotational Alignment. *Nano Lett* 2016, **16**(3)**:** 1989-1995.
25. Burzuri E, Vera-Hidalgo M, Giovanelli E, Villalva J, Castellanos-Gomez A, Perez EM. Simultaneous assembly of van der Waals heterostructures into multiple nanodevices. *Nanoscale* 2018, **10**(17)**:** 7966-7970.
26. Chen H, He J, Malliakas CD, Stoumpos CC, Rettie AJE, Bao J-K, *et al.* A Natural 2D Heterostructure [Pb3.1Sb0.9S4][AuxTe2–x] with Large Transverse Nonsaturating Negative Magnetoresistance and High Electron Mobility. *J Am Chem Soc* 2019, **141**(18)**:** 7544-7553.
27. Niu Y, Villalva J, Frisenda R, Sanchez-Santolino G, Ruiz-González L, Pérez EM, *et al.* Mechanical and liquid phase exfoliation of cylindrite: a natural van der Waals superlattice with intrinsic magnetic interactions. *2D Materials* 2019, **6**(3)**:** 035023.
28. Wang B, Zhong SP, Zhang ZB, Zheng ZQ, Zhang YP, Zhang H. Broadband photodetectors based on 2D group IVA metal chalcogenides semiconductors. *Applied Materials Today* 2019, **15:** 115-138.
29. Navarro JJ, Calleja F, Miranda R, Perez EM, Vazquez de Parga AL. High yielding and extremely site-selective covalent functionalization of graphene. *Chem Commun (Cambridge, U K)* 2017, **53**(75)**:** 10418-10421.
30. Navarro JJ, Leret S, Calleja F, Stradi D, Black A, Bernardo-Gavito R, *et al.* Organic Covalent Patterning of Nanostructured Graphene with Selectivity at the Atomic Level. *Nano Lett* 2016, **16**(1)**:** 355-361.
31. Makovicky E, Dušek M, Petříček V, Topa D. The crystal structure of franckeite, Pb21.7Sn9.3Fe4.0Sb8.1S56.9. *Am Mineral* 2011, **96**(11-12)**:** 1686-1702.
32. Ray K, Yore AE, Mou T, Jha S, Smithe KKH, Wang B, *et al.* Photoresponse of Natural van der Waals Heterostructures. *ACS Nano* 2017, **11:** 6024-6030.
33. Vera-Hidalgo M, Giovanelli E, Navio C, Perez EM. Mild Covalent Functionalization of Transition Metal Dichalcogenides with Maleimides: A "Click" Reaction for 2H-MoS2 and WS2. *J Am Chem Soc* 2019, **141**(9)**:** 3767-3771.
34. Molina-Mendoza AJ, Giovanelli E, Paz WS, Angel Nino M, Island JO, Evangeli C, *et al.* Franckeite as a naturally occurring van der Waals heterostructure. *Nat Comm* 2017, **8**.
35. Beckonert O, Coen M, Keun HC, Wang Y, Ebbels TMD, Holmes E, *et al.* High-resolution magic-angle-spinning NMR spectroscopy for metabolic profiling of intact tissues. *Nat Protoc* 2010, **5:** 1019.
36. T. M. Alam and J. E. Jenkins. HR-MAS NMR Spectroscopy in Material Science, Advanced Aspects of Spectroscopy, Ed. Muhammad Akhyar Farrukh, IntechOpen, DOI: 10.5772/48340. Available from: https://www.intechopen.com/books/advanced-aspects-of-spectroscopy/hr-mas-nmr-spectroscopy-in-material-science
37. Warrass R, Lippens G. Quantitative monitoring of solid phase organic reactions by high-resolution magic angle spinning NMR spectroscopy. *J Org Chem* 2000, **65**(10)**:** 2946-2950.
38. Pauling L. The nature of the chemical bond. III. The transition from one extreme bond type to another. *J Am Chem Soc* 1932, **54:** 988-1003.

39. In fact, adding a third component for the S 2p peak improves the fitting (Fig. S9) but considering our experimental resolution we do not think it is sufficiently justified.
40. Vacchi IA, Spinato C, Raya J, Bianco A, Menard-Moyon C. Chemical reactivity of graphene oxide towards amines elucidated by solid-state NMR. *Nanoscale* 2016, **8**(28)**:** 13714-13721.